

ANALYSIS OF THE DIVIDE-AND-CONQUER METHOD FOR ELECTRONIC STRUCTURE CALCULATIONS

JINGRUN CHEN AND JIANFENG LU

ABSTRACT. We study the accuracy of the divide-and-conquer method for electronic structure calculations. The analysis is conducted for a prototypical subdomain problem in the method. We prove that the pointwise difference between electron densities of the global system and the subsystem decays exponentially as a function of the distance away from the boundary of the subsystem, under the gap assumption of both the global system and the subsystem. We show that gap assumption is crucial for the accuracy of the divide-and-conquer method by numerical examples. In particular, we show examples with the loss of accuracy when the gap assumption of the subsystem is invalid.

1. INTRODUCTION

Many systems in materials science, chemistry and other areas are greatly influenced by the electronic structure, which requires the full quantum-mechanical description. However, directly solving the quantum many-body problem for real systems is impractical even with the present supercomputers since a $3N$ -dimensional antisymmetric wave function is needed to describe a system with N electrons. Lots of electronic structure models, which aim at approximating the solution of many-body Schrödinger equations, have been proposed.

Kohn-Sham density functional theory (DFT) [11, 14, 15, 17] is one of the most popular and successful tools for electronic structure analysis, in which N one-particle wave functions are used to describe the N -electron system with properly approximated energy functionals. The corresponding Kohn-Sham equations are a system of nonlinear eigenvalue problems. To solve the nonlinear eigenvalue equation, the self-consistent field iteration is often used. The electron density is updated at each iteration until self-consistency is achieved. The computational cost of each iteration step for conventional algorithm scales as $\mathcal{O}(N^3)$ due to diagonalization and orthogonalization. For different systems, the required number of iterations might scale differently and depends on the choice of mixing techniques. The total cost of solving the Kohn-Sham equations scales at least as $\mathcal{O}(N^3)$. Such computational scaling is prohibitively expensive when the number of electrons is large.

Many efforts have been devoted to design linear scaling methods, i.e., $\mathcal{O}(N)$ methods, for electronic calculations within the framework of Kohn-Sham DFT over the past twenty years (see e.g. [6, 10]). These methods share the common ground of exploiting the locality, or nearsightedness [13, 18] to reduce the computational complexity. Locality here means the dependence of the electron density on the environment decays in distance. The first linear scaling method is the divide-and-conquer (DAC) method proposed by Weitao Yang [22, 23], where the global system is

Date: April 7, 2015.

2000 Mathematics Subject Classification. 15A18, 35P99, 65N25.

Key words and phrases. Density functional theory, divide-and-conquer method, gap assumption, exponential decay.

divided into several subsystems, and each subsystem is solved separately with atomic orbitals. The electron density of the global system is then found by getting a global equilibrium condition for the Fermi energy. In each self-consistent iteration, the cost of DAC method depends on the number of subsystems which is proportional to the number of electrons. The DAC method scales as $\mathcal{O}(N)$ naturally if the self-consistent field iteration is independent of the considered system.

In this article, we aim at understanding the accuracy of the DAC method, as one of the popular approaches of linear scaling algorithms. We note that the main idea of the algorithm is quite similar to the domain decomposition type method, commonly used in numerical solutions to PDEs. The goal is to understand the accuracy of the method and the conditions under which the method works. A key component of the analysis is to understand the locality of electronic structure from a mathematical point of view. The main ingredients are geometric resolvent identity and a Combes-Thomas type decay estimate of the Green's function.

In the DAC method of electronic structure calculations, the subsystem can be understood as the global system under certain (not necessarily small) perturbations. It turns out that the accuracy of the method depends crucially on the gap structure of the system and of the subsystem. We examine the gap assumption in cases when it is valid and invalid carefully with numerous examples. Let us also point out that our analysis does not assume any particular way of restriction of the Hamiltonian onto a sub-domain (besides that the gap assumption is satisfied). This flexibility allows the analysis to be generalized to a variety of methods in electronic structure calculations based on the domain decomposition idea.

The outline of the paper is as follows. The detailed description of the DAC method is presented in §2. The accuracy of the method is analyzed in §3. By examples in one dimension and two dimensions, we demonstrate the accuracy of the method when the gap assumption is valid, and the loss of the accuracy when the gap assumption is invalid in §4.

2. DIVIDE-AND-CONQUER METHOD

2.1. Kohn-Sham density functional theory. Consider a system of N_c nuclei and N electrons. A set of one-particle wave functions $\{\psi_k(x)\}_{k=1}^N$ is employed to represent the interacting electrons in Kohn-Sham DFT. At zero temperature, the Kohn-Sham energy functional can be written as (for simplicity of the presentation, we will ignore the spin degeneracy here and in sequel)

$$(2.1) \quad E_{\text{KS}}[\{\psi_k\}_{k=1}^N] = \sum_{k=1}^N \int_{\mathbb{R}^3} \frac{1}{2} |\nabla \psi_k|^2 dx + \int_{\mathbb{R}^3} V(x) \rho(x) dx \\ + \frac{1}{2} \iint_{\mathbb{R}^3 \times \mathbb{R}^3} \frac{(\rho - m)(x)(\rho - m)(x')}{|x - x'|} dx dx' + E_{\text{XC}}[\rho],$$

where the electron density is given by

$$(2.2) \quad \rho(x) = \sum_{k=1}^N |\psi_k(x)|^2,$$

and the ionic function takes the form

$$(2.3) \quad m(x) = \sum_{k=1}^{N_c} m^a(x - R_k),$$

where m^a is a localized smooth function and $\{R_k\}_{k=1}^{N_c}$ are the positions of nuclei, i.e., we have taken a local pseudopotential for the electron-nucleus interaction [15] for simplicity. Our results can be generalized to nonlocal pseudopotential, but we will not go into the details.

The Kohn-Sham energy functional is minimized with the orthonormal constraints of the orbitals

$$(2.4) \quad \int_{\mathbb{R}^3} \psi_k(x)\psi_l(x)dx = \delta_{kl}, \quad k, l = 1, 2, \dots, N.$$

The Euler-Lagrange equation, known as the Kohn-Sham equation, can be written as

$$(2.5) \quad H(\rho)\psi_k(x) = \epsilon_k\psi_k(x), \quad k = 1, 2, \dots, N,$$

where $H(\rho) = -\frac{1}{2}\Delta + V_{\text{eff}}$ with $V_{\text{eff}} = V(x) + \int_{\mathbb{R}^3} \frac{\rho(x') - m(x')}{|x-x'|} dx' + V_{\text{XC}}[\rho]$ and $V_{\text{XC}}[\rho] = \frac{\delta E_{\text{XC}}[\rho]}{\delta \rho}$. Here, ϵ_k are a set of eigenvalues, increasingly ordered, and $\{\psi_k\}$ are the associated eigenfunctions of the effective Hamiltonian. Note that this is a nonlinear eigenvalue problem as the effective Hamiltonian H depends on the density, which in turn, depends on the eigenfunctions.

To solve the Kohn-Sham equation (2.5), a self-consistent iteration is usually employed. At each iterate, for the current guess of the density ρ , we solve for the eigenvalue problem of $H(\rho)$ to find the first N eigenpairs $\{\epsilon_k, \psi_k\}$. From the eigenfunctions, we form a new density $\rho_{\text{new}} = \sum_k |\psi_k|^2$. The nonlinear iteration is used to find a fixed point of the map from ρ to ρ_{new} , which is known as the Kohn-Sham map (see e.g., [8]).

The algorithmic bottleneck of the above procedure is to evaluate the density ρ_{new} given a Hamiltonian: For a fixed Hamiltonian $H = -\frac{1}{2}\Delta + V(x)$ with some effective potential $V \in L^\infty$ (consequently, we will take $\mathcal{D}(H) = H^2(\mathbb{R}^3)$), we look for the square sum of its first N eigenfunctions,

$$(2.6) \quad H\psi_k(x) = \epsilon_k\psi_k(x), \quad k = 1, \dots, N,$$

which is a linear eigenvalue problem. A conventional diagonalization of the discretized Hamiltonian to solve (2.6) leads to computational cost that scales cubically with respect to the number of electrons. However, the eigenfunctions $\{\psi_k\}$ are just an intermediate step for the electron density $\rho = \sum_k |\psi_k|^2$. It is therefore possible to design efficient algorithms that avoid the eigenvalue problem on the whole computational domain. One such strategy is the DAC method, which aims to achieve linear scaling cost for computing the density.

2.2. Divide-and-conquer method. The idea of using the DAC method to study electron structures was firstly proposed by Weitao Yang in [22, 23], which was based on a localized Hamiltonian formulation. It was then generalized to a density-matrix formulation [24]. Some recent developments of the DAC method, or more generally, domain decomposition type method, can be found in [3, 4, 21, 25]. A great advantage of the method lies on the intrinsic parallel properties between subdomains, which has been investigated for large scale calculations with more than 10^6 atoms and 10^{12} electronic degrees of freedom [12, 16, 19, 20]. In what follows, we describe the main idea of the DAC method, in the spirit of [22]. To clearly present the method, we will stay on the PDE level and formulate the algorithm in terms of operators, rather than first imposing a discretization of the Hamiltonian. This way, we can separate the error caused by the DAC method and by a numerical discretization of the continuous problem.

The DAC method for electronic structure calculations involves the following steps. Let us denote the whole computational domain as Ω . Our goal is to find its corresponding density of the Hamiltonian H on the whole domain.

- Step 1. Define a partition of domain, $\{\Lambda_\alpha\}$, and a partition of unity subordinate to the open covering $\{\Lambda_\alpha, p_\alpha\}$. Usually neighboring subdomains intersect, i.e., $\Lambda_\alpha \cap \Lambda_{\alpha'} \neq \emptyset$ when $\alpha \neq \alpha'$. Nonnegative partition functions $\{p_\alpha\}$ satisfy $\sum_\alpha p_\alpha(x) = 1, \forall x \in \Omega$.
- Step 2. Restrict the Hamiltonian on the domain Λ_α with certain boundary conditions and solve the eigenvalue problem in each subsystem

$$(2.7) \quad H_{\Lambda_\alpha} \psi_k^\alpha(x) = \epsilon_k^\alpha \psi_k^\alpha(x), \quad x \in \Lambda_\alpha,$$

where H_{Λ_α} denotes the restriction of the Hamiltonian, whose domain is a subset of the Sobolev space $H^2(\Lambda_\alpha)$ with prescribed boundary conditions.

- Step 3. Determine the Fermi energy ϵ_F by solving the equation of charge equilibrium

$$(2.8) \quad N = \sum_\alpha \sum_k f_\beta(\epsilon_F - \epsilon_k^\alpha) \int_{\Lambda_\alpha} p_\alpha(x) |\psi_k^\alpha(x)|^2 dx,$$

where $f_\beta(\epsilon) = (1 + e^{\beta(\epsilon - \epsilon_F)})^{-1}$ is the Fermi-Dirac function and $\beta = \frac{1}{k_B T}$ with k_B Boltzmann constant and T absolute temperature.

- Step 4. Construct the electron density

$$(2.9) \quad \rho^{\text{DAC}}(x) = \sum_\alpha p_\alpha(x) \rho_\alpha(x),$$

where $\rho_\alpha(x) = \sum_k f_\beta(\epsilon_F - \epsilon_k^\alpha) |\psi_k^\alpha(x)|^2$, and total energy

$$(2.10) \quad \begin{aligned} E = & \sum_\alpha \sum_k \epsilon_k^\alpha f_\beta(\epsilon_F - \epsilon_k^\alpha) \int_{\Lambda_\alpha} p_\alpha(x) |\psi_k^\alpha(x)|^2 dx - \frac{1}{2} \int_\Omega \int_\Omega \frac{\rho^{\text{DAC}}(x) \rho^{\text{DAC}}(x')}{|x - x'|} dx dx' \\ & + \frac{1}{2} \int_\Omega \int_\Omega \frac{m(x)m(x')}{|x - x'|} dx dx' - \int_\Omega V_{\text{XC}}[\rho^{\text{DAC}}] \rho^{\text{DAC}}(x) dx + E_{\text{XC}}[\rho^{\text{DAC}}]. \end{aligned}$$

Note that the above formulation corresponds to a finite temperature calculation, as considered in the original DAC method [22]. In practice, if interested in the zero temperature calculation, we may choose β so large that the Fermi-Dirac function becomes approximately a Heaviside function. In the following analysis and numerical examples, we will consider the zero temperature case to focus on the key idea. Our analysis can be extended to finite temperature situation.

2.3. A prototypical subsystem problem. From an analytical point of view, we can just focus on one subsystem problem from the divide-and-conquer method. The analysis for other subdomains proceeds in the same fashion and the error of the method over the whole domain can be controlled by those of the sub-domains using triangle inequality and observing that p_α is a partition of unity. More specifically, note that the global density in the DAC method is obtained by $\rho^{\text{DAC}}(x) = \sum_\alpha p_\alpha(x) \rho_\alpha(x)$ where ρ_α is the electron density calculated in Λ_α . Denoting ρ the true density, we have

$$\begin{aligned} \|\rho - \rho^{\text{DAC}}\|_{L^\infty} &= \sup_x \left| \sum_\alpha p_\alpha(x) (\rho(x) - \rho_\alpha(x)) \right| \\ &\leq \sup_\alpha \|\rho - \rho_\alpha\|_{L^\infty(\Lambda_\alpha)}. \end{aligned}$$

Error estimate in other norms can be similarly obtained.

Let us reformulate the DAC idea for a single domain. Let Λ be a subdomain and let Λ_b be a buffer region surrounding Λ . In terms of the algorithm in the previous section, Λ_b corresponds to one of the $\{\Lambda_\alpha\}$, and Λ is the support of p_α , which we choose to be strictly inside. Later in the analysis, we will also need a slightly smaller buffer region $\tilde{\Lambda}_b$ inside of Λ_b . These sets satisfy $\Lambda \subset \tilde{\Lambda}_b \subset \Lambda_b \subset \Omega$ with some distance separating their boundaries, see Figure 1(a) for a schematic picture.

For a prescribed Fermi energy ϵ_F , we are interested in the density over the domain Λ , calculated by solving the eigenproblem on Λ_b . Namely, we define

$$(2.11) \quad \rho_\Lambda(x) = \sum_{\epsilon_k \leq \epsilon_F} |\psi_k(x)|^2, \quad x \in \Lambda,$$

where the eigenpairs (ϵ_k, ψ_k) are obtained by solving the following eigenvalue problem in Λ_b

$$(2.12) \quad H_{\Lambda_b} \psi_k = \epsilon_k \psi_k, \quad k = 1, 2, \dots$$

To understand the accuracy of the DAC method, it then suffices to understand the difference between ρ_Λ and the exact density ρ restricted on Λ .

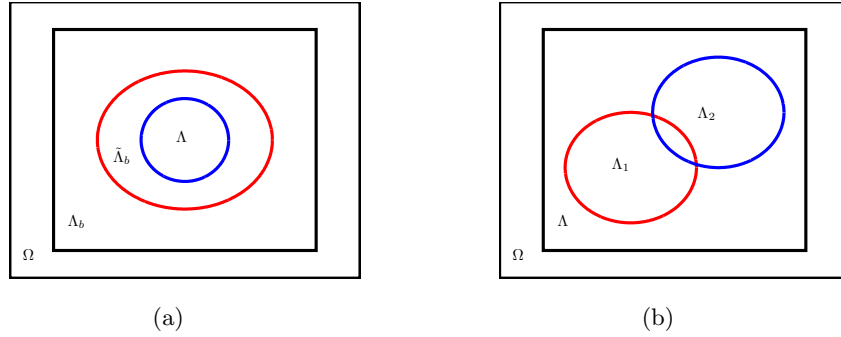


FIGURE 1. Schematic pictures of domain and subdomains in the DAC method and the geometric resolvent identity. (a) A prototypical subdomain problem in the DAC method; (b) Domain and subdomains in the geometric resolvent identity Lemma 3.1.

3. ACCURACY OF THE METHOD

The main tool we will use is the geometric resolvent identity and the decay estimate of the Green's functions. The geometric resolvent identity relates the Green's function defined on a subdomain to the Green's function on a larger domain. For a domain Λ , we will denote Λ^c its complement; and for two sets A and B , $\text{dist}(A, B) = \inf_{x \in A, y \in B} \text{dist}(x, y)$.

Lemma 3.1 (Geometric Resolvent Identity). *Consider four open sets $\Lambda_1, \Lambda_2, \Lambda$ and Ω that satisfy $\Lambda_1 \subset \Lambda, \Lambda_2 \subset \Lambda, \Lambda \subset \Omega$ and $\text{dist}\{\Lambda_1 \cup \Lambda_2, \Lambda^c\} > 0$ (see Figure 1(b) for an illustration of these sets). Let Θ be a smooth function which is identically 1 on a neighborhood of $\Lambda_1 \cup \Lambda_2$ and identically 0 on a neighborhood of Λ^c . Given any restriction H_Ω and H_Λ of H to Ω and Λ , respectively, we have*

$$(3.1) \quad 1_{\Lambda_1}(H_\Omega - \lambda)^{-1} = 1_{\Lambda_1}(H_\Lambda - \lambda)^{-1}\Theta + 1_{\Lambda_1}(H_\Lambda - \lambda)^{-1}[H, \Theta](H_\Omega - \lambda)^{-1}$$

for any λ for which both resolvents exist. Also

$$(3.2) \quad 1_{\Lambda_1}(H_\Omega - \lambda)^{-1}1_{\Lambda_2} = 1_{\Lambda_1}(H_\Lambda - \lambda)^{-1}1_{\Lambda_2} + 1_{\Lambda_1}(H_\Lambda - \lambda)^{-1}[H, \Theta](H_\Omega - \lambda)^{-1}1_{\Lambda_2},$$

under the same conditions.

Proof. The lemma is well-known in the analysis of Schrödinger operators and its proof is standard (see e.g., [2, Lemma 4.2]). We include the short proof here for completeness. First note the identity

$$(3.3) \quad [H, \Theta] = (H_\Lambda - \lambda)\Theta - \Theta(H_\Omega - \lambda)$$

since $\text{supp } \Theta \subset \Lambda \subset \Omega$. The identity (3.1) follows from multiplying on the left by $1_{\Lambda_1}(H_\Omega - \lambda)^{-1}$ and on the right by $(H_\Omega - \lambda)^{-1}$. The identity (3.2) follows from (3.1) by applying 1_{Λ_2} on the right on both hand sides. \square

Let us recall the spectral representation of the electron density (see e.g., [8])

$$(3.4) \quad \rho(x) = \frac{1}{2\pi i} \int_{\mathcal{C}} (\lambda - H)^{-1} d\lambda(x, x),$$

where the right hand side stands for the diagonal of the kernel of the operator $(2\pi i)^{-1} \int_{\mathcal{C}} (\lambda - H)^{-1} d\lambda$. Here \mathcal{C} is a contour in the complex plane that separates the occupied spectrum of H (the eigenvalues below the Fermi energy ϵ_F with the rest of the spectrum). In the DAC method, this is approximated by

$$(3.5) \quad \rho_\Lambda(x) = \frac{1}{2\pi i} \int_{\mathcal{C}} (\lambda - H_{\Lambda_b})^{-1} d\lambda(x, x),$$

where Λ_b is a buffer region surrounding Λ . Without loss of generality, we will assume that the buffer satisfies $\text{dist}(\Lambda, \Lambda_b^c) \geq 2$. We will also define the region

$$(3.6) \quad \tilde{\Lambda}_b = \{x \in \Lambda_b \mid \text{dist}(x, \Lambda_b^c) \leq 1\}.$$

By construction, it is clear that we have $\text{dist}(\Lambda, \tilde{\Lambda}_b^c) \geq 1$. We note that the distances 1 and 2 are chosen here merely for convenience, any finite $\mathcal{O}(1)$ distance will work, though the final constants in the estimate depend on how separated the domains are.

We may proceed to compare the pointwise values of ρ and ρ_Λ by using results on regularity estimate of Green's function for elliptic operators (e.g., [1] and [8, Lemma 6.4]). Here, for simplicity of presentation and to better convey the key idea, we will instead work with the following locally mollified version of the densities (with slight abuse of notations, we still denote them as ρ and ρ_Λ)

$$(3.7) \quad \rho(x) = \frac{1}{2\pi i} \int_{\mathcal{C}} \langle \varphi_x, (\lambda - H)^{-1} \varphi_x \rangle d\lambda,$$

$$(3.8) \quad \rho_\Lambda(x) = \frac{1}{2\pi i} \int_{\mathcal{C}} \langle \varphi_x, (\lambda - H_{\Lambda_b})^{-1} \varphi_x \rangle d\lambda,$$

where φ_x is a fixed numerical delta function centered at x . For simplicity of notation, we will also abuse the notation by writing $\text{dist}(x, A) := \text{dist}(\text{supp } \varphi_x, A)$ for a set A . Note that the mollification is in agreement with practical numerical implementations, since some discretization will be used for the Hamiltonian operator. Other forms of φ_x , such as averaging in a small ball around x , can also be used. Accuracy of the method is the same with a possibly different constant.

In general, the restriction of H onto the domain Λ_b might dramatically change the spectrum of the operator. As will be shown in the numerical examples, without any assumption on the spectral properties of the truncated operator H_{Λ_b} , the accuracy of the method is not guaranteed, in particular, the difference between $\rho(x)$ and $\rho_{\Lambda}(x)$ might be quite large and decay very slowly when x is moving inside Λ away from the boundary $\partial\Lambda$. To guarantee the fast decay of the error, we make the following gap assumption for the truncated system H_{Λ_b} .

Assumption A (Gap assumption). Let $\text{spec}_{\text{occ}}(H)$ and $\text{spec}_{\text{unocc}}(H)$ be the occupied and unoccupied spectra of H respectively. We assume that there exists ϵ_F and $e_g > 0$ such that

$$(3.9) \quad \epsilon_F - e_g/2 \geq \sup \text{spec}_{\text{occ}}(H);$$

$$(3.10) \quad \epsilon_F + e_g/2 \leq \inf \text{spec}_{\text{unocc}}(H);$$

$$(3.11) \quad (\epsilon_F - e_g/2, \epsilon_F + e_g/2) \cap \text{spec}(H_{\Lambda_b}) = \emptyset.$$

Note that, e_g might be smaller than the spectral gap between occupied and unoccupied spectra of H . Physically, the assumption means that the restriction of the Hamiltonian operator on the subsystem preserves the gap around the Fermi energy. In particular, the assumption implies the existence of a contour \mathcal{C} such that

$$\text{dist}(\mathcal{C}, \text{spec}(H)) \geq e_g/2 \quad \text{and} \quad \text{dist}(\mathcal{C}, \text{spec}(H_{\Lambda_b})) \geq e_g/2.$$

Remark. If Assumption A is satisfied by all the sub-domains, we can then find a uniform gap in the spectra of all sub-domain Hamiltonians. This means that the Fermi level can be chosen uniformly for all the sub-domain, which gives the choice of the global Fermi energy in Step 3 of the DAC algorithm.

Theorem 3.2 (Accuracy of the method). *Under Assumption A, there exist constants C and γ such that*

$$(3.12) \quad |\rho(x) - \rho_{\Lambda}(x)| \leq C e^{-2\gamma(\text{dist}(x, \Lambda_b^c) - 1)}, \quad \forall x \in \Lambda.$$

The constants C and γ depend only on ϵ_F , e_g and $\|V\|_{L^\infty}$.

Remark. The estimate (3.12) guarantees that with a fixed buffer region, the error we make by restricting to a local problem decays exponentially away from the boundary. As the constants depend only on the spectral gap and the L^∞ norm of the potential, if we fix a point x and enlarge the buffer region Λ_b , the error will also decay exponentially, as long as the gap assumption is uniformly satisfied for the increasing buffer regions. This point would be further demonstrated in the numerical examples.

Before we prove the theorem, let us recall the decay estimate of Green's function from [7, Theorem 9] and its proof (see also [8] where such estimates are used for the macroscopic limit of Kohn-Sham density functional theory). We also remark that the exponential decay property of the Green's function and the density matrix also holds at the discrete level [5] and hence our analysis can be also done for the discretized Hamiltonian.

Proposition 3.3 (Decay estimate of Green's function). *Given a Hamiltonian $H = -\Delta + V$ with $V \in L^\infty$. For any $\lambda \notin \text{spec}(H)$, there exist constants $\gamma_{\max} > 0$ and M , depending only on $\text{dist}(\lambda, \text{spec}(H))$, $|\lambda|$ and $\|V\|_{L^\infty}$, such that for all x_0 and any $\gamma < \gamma_{\max}$, we have*

$$(3.13) \quad \|\mathcal{W}_{x_0}^{-1}(\lambda - H)^{-1}\mathcal{W}_{x_0}\| \leq M$$

$$(3.14) \quad \|\mathcal{W}_{x_0}^{-1}\partial_j(\lambda - H)^{-1}\mathcal{W}_{x_0}\| \leq M, \quad \text{for } j = 1, \dots, d,$$

where d is the dimension, and \mathcal{W}_{x_0} is the multiplication operator given by

$$(3.15) \quad (\mathcal{W}_{x_0}f)(x) = \exp(-\gamma((x - x_0)^2 + 1)^{1/2})f(x).$$

Applying the result to our current setting, since \mathcal{C} is compact and by the gap assumption, $\text{dist}(\mathcal{C}, \text{spec}(H)), \text{dist}(\mathcal{C}, \text{spec}(H_{\Lambda_d})) > e_g/2$, the γ_{\max} and M can be chosen for both H and H_{Λ_b} as constants depending only on \mathcal{C}, e_g , and $\|V\|_{L^\infty}$. Moreover, the choice of the contour only depend on the location of the spectral gap and the bottom of the spectra of H and H_{Λ_b} , which can be controlled by ϵ_F and $\|V\|_{L^\infty}$. Hence, the constants only depend on ϵ_F, e_g and $\|V\|_{L^\infty}$. Let us now proceed to prove the Theorem.

Proof of Theorem 3.2. Using the resolvent identity, we write the difference in density as the difference in operators. For $x \in \Lambda$, we have

$$\rho(x) - \rho_\Lambda(x) = \frac{1}{2\pi i} \int_{\mathcal{C}} \langle \varphi_x, [(\lambda - H)^{-1} - (\lambda - H_{\Lambda_b})^{-1}] \varphi_x \rangle d\lambda$$

Since the contour \mathcal{C} is compact, we obtain

$$|\rho(x) - \rho_\Lambda(x)| \lesssim \max_{\lambda \in \mathcal{C}} \left| \langle \varphi_x, [(\lambda - H)^{-1} - (\lambda - H_{\Lambda_b})^{-1}] \varphi_x \rangle \right|.$$

Let Λ_x denote the support of φ_x , using Lemma 3.1, we have the geometric resolvent identity

$$(3.16) \quad 1_{\Lambda_x} [(\lambda - H)^{-1} - (\lambda - H_{\Lambda_b})^{-1}] 1_{\Lambda_x} = 1_{\Lambda_x} (\lambda - H_{\Lambda_b})^{-1} [H, \Theta] (\lambda - H)^{-1} 1_{\Lambda_x},$$

where we take Θ such that $\Theta = 1$ in $\tilde{\Lambda}_b$ and $\Theta = 0$ outside Λ_b . The commutator $[H, \Theta]$ can be calculated as

$$[H, \Theta] = -(\Delta\Theta) - 2\nabla\Theta \cdot \nabla.$$

Note that both $\Delta\Theta$ and $\nabla\Theta$ are supported on $\Lambda_b \setminus \tilde{\Lambda}_b$ by the choice of Θ . By the construction of the set $\tilde{\Lambda}_b$ as in (3.6), we can choose Θ such that $\|\Delta\Theta\|_{L^\infty}$ and $\|\nabla\Theta\|_{L^\infty}$ are both $\mathcal{O}(1)$ quantities. Applying (3.16), we hence arrive at

$$\begin{aligned} \left| \langle \varphi_x, [(\lambda - H)^{-1} - (\lambda - H_{\Lambda_b})^{-1}] \varphi_x \rangle \right| &\leq \left| \langle \varphi_x, (\lambda - H_{\Lambda_b})^{-1} (\Delta\Theta) (\lambda - H)^{-1} \varphi_x \rangle \right| \\ &\quad + 2 \left| \langle \varphi_x, (\lambda - H_{\Lambda_b})^{-1} (\nabla\Theta \cdot \nabla) (\lambda - H)^{-1} \varphi_x \rangle \right|. \end{aligned}$$

The proof then concludes by estimating the two terms on the right hand side. These decay estimates are given by the next Lemma 3.4. \square

Lemma 3.4 (Decay estimates). *Let f be a L^∞ function such that*

$$\text{supp } f \subset \Lambda_b \setminus \tilde{\Lambda}_b.$$

There exist constants $\gamma_{\max} > 0$ and C such that for any $\lambda \in \mathcal{C}$ and $\gamma < \gamma_{\max}$, we have

$$(3.17) \quad \left| \langle \varphi_x, (\lambda - H_{\Lambda_b})^{-1} f(\lambda - H)^{-1} \varphi_x \rangle \right| \leq C \exp(-2\gamma(\text{dist}(x, \Lambda_b^c) - 1)) \|f\|_{L^\infty};$$

$$(3.18) \quad \left| \langle \varphi_x, (\lambda - H_{\Lambda_b})^{-1} f \partial_j (\lambda - H)^{-1} \varphi_x \rangle \right| \leq C \exp(-2\gamma(\text{dist}(x, \Lambda_b^c) - 1)) \|f\|_{L^\infty}.$$

where f is interpreted as a multiplication operator on the left hand sides.

Proof. By inserting the exponential weight \mathcal{W}_x centered at x , we can estimate

$$\begin{aligned} & \left| \langle \varphi_x, (\lambda - H_{\Lambda_b})^{-1} f(\lambda - H)^{-1} \varphi_x \rangle \right| \\ &= \left| \langle (\lambda - H_{\Lambda_b})^{-1} \varphi_x, f(\lambda - H)^{-1} \varphi_x \rangle \right| \\ &= \left| \langle \mathcal{W}_x^{-1} (\lambda - H_{\Lambda_b})^{-1} \mathcal{W}_x \mathcal{W}_x^{-1} \varphi_x, \mathcal{W}_x f \mathcal{W}_x \mathcal{W}_x^{-1} (\lambda - H)^{-1} \mathcal{W}_x \mathcal{W}_x^{-1} \varphi_x \rangle \right| \\ &\leq \| \mathcal{W}_x^{-1} \varphi_x \|_{L^2}^2 \| \mathcal{W}_x^{-1} (\lambda - H_{\Lambda_b})^{-1} \mathcal{W}_x \| \| \mathcal{W}_x^{-1} (\lambda - H)^{-1} \mathcal{W}_x \| \| \mathcal{W}_x f \mathcal{W}_x \| \\ &\lesssim \| \mathcal{W}_x f \mathcal{W}_x \|, \end{aligned}$$

where the last inequality uses Proposition 3.3 for the operators H and H_{Λ_b} . Note that $\mathcal{W}_x f \mathcal{W}_x$ is a multiplication operator

$$((\mathcal{W}_x f \mathcal{W}_x)u)(y) = \exp(-2\gamma((x - y)^2 + 1)^{1/2}) f(y)u(y),$$

Hence,

$$\begin{aligned} \| \mathcal{W}_x f \mathcal{W}_x \| &= \left\| \exp(-2\gamma((x - \cdot)^2 + 1)^{1/2}) f(\cdot) \right\|_{L^\infty} \\ &\leq \exp(-2\gamma(\text{dist}(x, \text{supp } f)^2 + 1)^{1/2}) \|f\|_{L^\infty} \\ &\leq \exp(-2\gamma(\text{dist}(x, \Lambda_b^c) - 1)) \|f\|_{L^\infty}. \end{aligned}$$

The proof of (3.18) is analogous and will be omitted. \square

4. GAP ASSUMPTION ON THE SUBSYSTEM

In this section, we validate the DAC algorithm and also our analytical results by numerical examples. By several examples in one dimension and two dimensions, we show the accuracy of the subsystem if Assumption A is valid. Moreover, the loss of accuracy for the subsystem is observed if Assumption A fails. While in practice, we do not have easy criteria of selection of subdomains that guarantees (3.9)–(3.11), numerical results show that they are essential for the accuracy of the method.

Example 4.1. Consider an infinite array of atoms on a line with $X_i = i$, for $i \in \mathbb{Z}$. Each atom has one valence electron and spin degeneracy is ignored. We adopt an example from [9], where V is chosen with the following form

$$V(x) = - \sum_{i \in \mathbb{Z}} \frac{a}{\sqrt{2\pi\sigma^2}} \exp[-(x - X_i)^2/2\sigma^2].$$

Figure 2 shows band structures when $a = 5$, $\sigma = 0.15$, and $a = 5$, $\sigma = 0.45$. We will assume one electron per atom (note that spin degeneracy is ignored). As studied in [9], the gap is very small when $a = 5$, $\sigma = 0.45$ and the system behaves like a metal. Therefore, it is clear that for selected parameters, the corresponding system has a gap in the spectrum (insulator) as in Figure 2(a),

while it does not have a gap (metal) as in Figure 2(b). In other words, (3.9)–(3.10) are valid in Figure 2(a), and invalid in Figure 2(b).

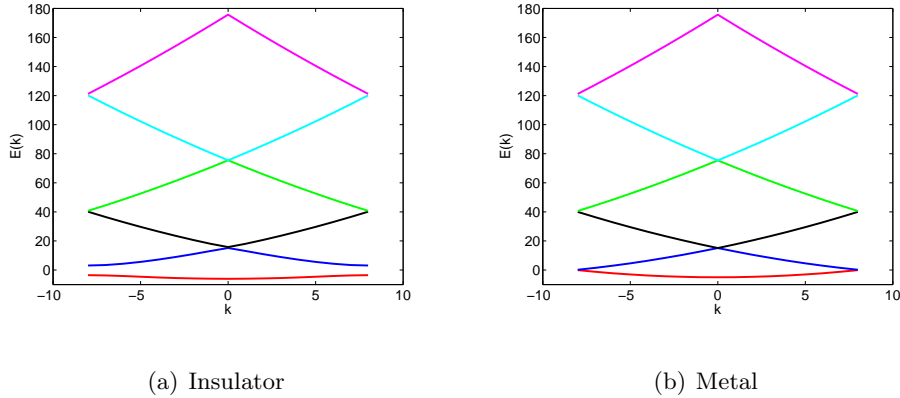


FIGURE 2. Band structures for different parameters in **Example 4.1**. The first band is occupied. (a) Insulator, where $a = 5$ and $\sigma = 0.15$; (b) Metal, where $a = 5$ and $\sigma = 0.45$.

Choose $\Omega = \mathbb{R}$ and $\Lambda_b = [0, 16]$. From the left column of Figure 3, one can see (3.11) is valid for H_{Λ_b} with three different boundary conditions, including Dirichlet boundary condition (DBC), Neumann boundary condition (NBC), and periodic boundary condition (PBC). Fix $\epsilon_F = (\epsilon_{\text{occ}} + \epsilon_{\text{unocc}})/2$ and $\Lambda = [0.1, 15.9]$. Note that $\text{dist}(\Lambda, \Lambda_b^c) \geq 0.1$, satisfying the assumption on the subdomain and the buffer region. This condition holds true for all examples in the section. We compare $|\rho(x) - \rho_\Lambda(x)|$ as a function of x for three boundary conditions in the right column of Figure 3. Density differences are plotted in the log scale and decay exponentially, which verifies (3.12). Quantitatively, the method has the best performance when PBC is used. Moreover, for the self-consistent Fermi level, density differences behave in the same manner.

Furthermore, for $\Lambda = [0, 16]$ and a series of enlarged buffer regions $\Lambda_b = [0 - x, 16 + x]$ ($x \geq 0.1$), we compare $|\rho(0) - \rho_\Lambda(0)|$ as a function of x in Figure 4. Density differences are plotted in the log scale and decay exponentially, since (3.11) is valid for the series of Λ_b .

Example 4.2. We now choose $a = 5$ and $\sigma = 0.45$ such that (3.9)–(3.10) are invalid as shown in Figure 2(b). Set $\Lambda_b = [0, 16]$ and $\Lambda = [0.1, 15.9]$. From the left column of Figure 5, one can see (3.11) is invalid for H_{Λ_b} with all three boundary conditions. Fix $\epsilon_F = (\epsilon_{\text{occ}} + \epsilon_{\text{unocc}})/2$. We compare $|\rho(x) - \rho_\Lambda(x)|$ as a function of x in the log-log scale for three boundary conditions in the right column of Figure 5. Density differences decay algebraically since Assumption A fails. Quantitatively, the method has the best performance when PBC is used.

Furthermore, for $\Lambda = [0, 16]$ and a series of enlarged buffer regions $\Lambda_b = [0 - x, 16 + x]$ ($x \geq 0.1$), we compare $|\rho(0) - \rho_\Lambda(0)|$ as a function of x in the log-log scale in Figure 6. Density differences decay algebraically as a result of the invalidity of (3.11) for the series of Λ_b .

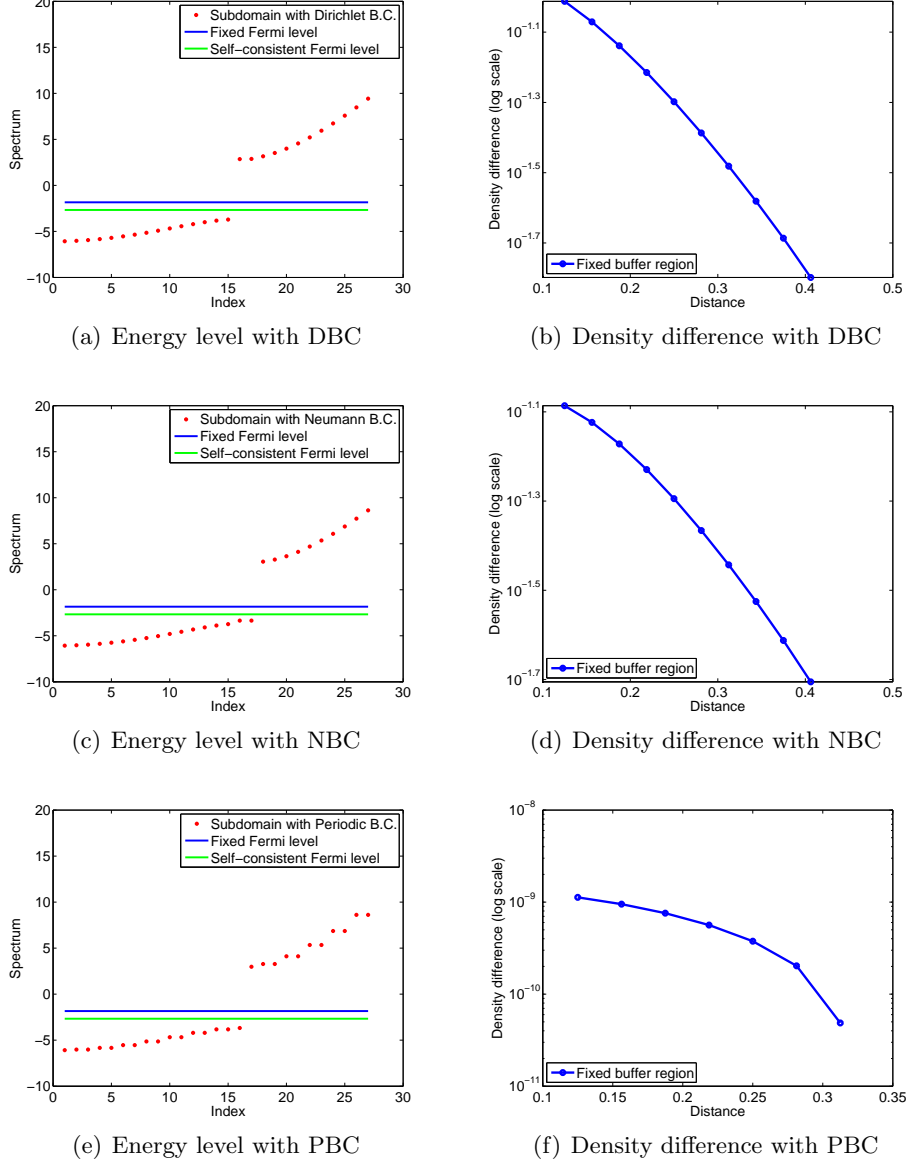
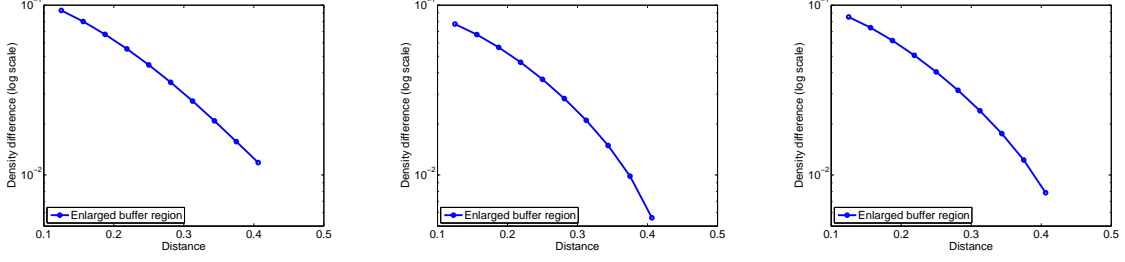


FIGURE 3. Energy levels of the subsystem, and $|\rho(x) - \rho_\Lambda(x)|$ as a function of x for $\Lambda = [0.1, 15.9]$ and $\Lambda_b = [0, 16]$ with different boundary conditions in **Example 4.1**. (a) Energy level with DBC; (b) Density difference with DBC; (c) Energy level with NBC; (d) Density difference with NBC; (e) Energy level with PBC; (f) Density difference with PBC. In the left column, red dots denote energy levels of the subsystem, blue line denotes the fixed Fermi level $\epsilon_F = (\epsilon_{\text{occ}} + \epsilon_{\text{unocc}})/2$, and green line denotes Fermi level obtained by the DAC method in a self-consistent manner, respectively. In the right column, density difference is plotted in the log scale and decays exponentially, which verifies (3.12).

Example 4.3 (Insulating global system, gap assumption invalid for the subsystem). For the next example, consider

$$V(x) = \begin{cases} -a, & 0 \leq x \leq 8; \\ -b, & 8 < x < 16; \\ \text{periodic extension,} & \text{otherwise.} \end{cases}$$



(a) Density difference with DBC (b) Density difference with NBC (c) Density difference with PBC

FIGURE 4. $|\rho(0) - \rho_\Lambda(0)|$ as a function of x for $\Lambda = [0, 16]$ and a series of enlarged buffer regions $\Lambda_b = [0-x, 16+x]$ ($x \geq 0.1$) with different boundary conditions in **Example 4.1**. (a) Density difference with DBC; (b) Density difference with NBC; (c) Density difference with PBC. Density difference is plotted in the log scale. Exponential decay rates are observed in all cases since Assumption A is valid.

We take $a = 5$ and $b = 0$ and plot the band structure of this problem in Figure 7(a). It is clear that this system is an insulating system.

First, we fix $\Lambda = [0.1, 7.9]$ and choose $\Lambda_b = [0, 8]$. Since $a = -5$, the subsystem is essentially an eigenvalue problem of the Laplacian operator, which means (3.11) is not valid; see Figure 7(b). Figure 8(a) shows that only algebraic decay rate is observed, since (3.9)–(3.10) are valid while (3.11) is invalid. Second, for the fixed $\Lambda = [3, 5]$, we choose a series of enlarged buffer regions $\Lambda_b = [3-x, 5+x]$ ($x \geq 0.1$) by varying x . $|\rho(5) - \rho_\Lambda(5)|$ as a function of x is shown in Figure 8(b). Algebraic decay rate is also observed since (3.11) is invalid in this case. Finally, we fix $\Lambda = [0, 8]$ and choose a series of enlarged buffer regions $\Lambda_b = [0-x, 8+x]$ ($x \geq 0.1$) by varying x . $|\rho(8) - \rho_\Lambda(8)|$ as a function of x is shown in Figure 8(c). Exponential decay rate is observed since (3.11) becomes valid in this case.

Example 4.4. Consider an infinite array of atoms on a two-dimensional lattice with $X_i = i, Y_j = j$, for $i \in \mathbb{Z}, j \in \mathbb{Z}$. Each atom has one valence electron and spin degeneracy is ignored. V is of the following form

$$V(x, y) = - \sum_{i \in \mathbb{Z}, j \in \mathbb{Z}} \frac{a}{\sqrt{2\pi\sigma^2}} \exp[-(x - X_i)^2/2\sigma^2 - (y - Y_j)^2/2\sigma^2].$$

Figure 9 shows band structures when $a = 10, \sigma = 0.15$, and $a = 10, \sigma = 0.45$. It is clear that for selected parameters, the corresponding system is an insulator in Figure 9(a), while it is a metal in Figure 9(b).

First, we fix $\Lambda = [0.1, 5.9] \times [0.1, 5.9]$ and choose $\Lambda_b = [0, 6] \times [0, 6]$. All three boundary conditions are tested. $|\rho(x) - \rho_\Lambda(x)|$ is plotted in the centered row of Figure 10 for DBC and PBC. Second, for the fixed $\Lambda = [2, 4] \times [2, 4]$, we consider a series of enlarged buffer regions $\Lambda_b = [2-x, 4+x] \times [2-x, 4+x]$ ($x \geq 0.1$). $|\rho(2, 2) - \rho_\Lambda(2, 2)|$ is plotted in the bottom row of Figure 10. The left column of Figure 10 is for the insulator case, while the right column is for the metal case. Results here are consistent with theoretical estimates.

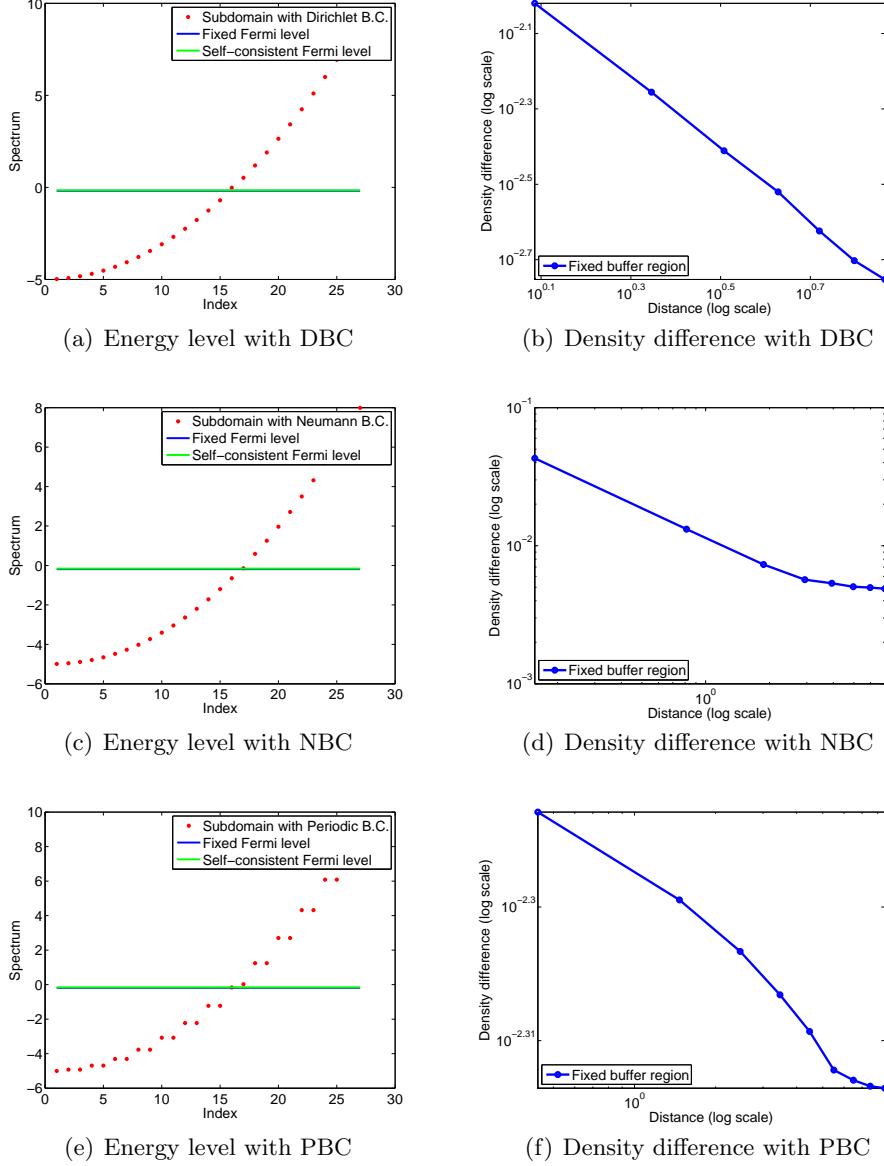
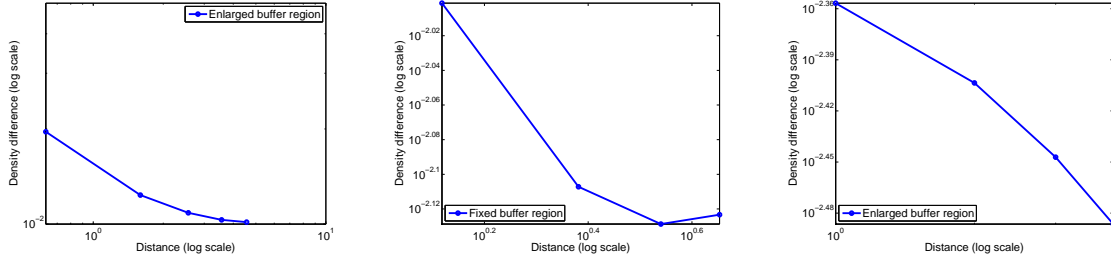


FIGURE 5. Energy levels of the subsystem, and $|\rho(x) - \rho_\Lambda(x)|$ as a function of x in the log-log scale for $\Lambda = [0.1, 15.9]$ and $\Lambda_b = [0, 16]$ with different boundary conditions in **Example 4.2**. (a) Energy level with DBC; (b) Density difference with DBC; (c) Energy level with NBC; (d) Density difference with NBC; (e) Energy level with PBC; (f) Density difference with PBC. In the left column, red dots denote energy levels of the subsystem, blue line denotes the fixed Fermi level $\epsilon_F = (\epsilon_{\text{occ}} + \epsilon_{\text{unocc}})/2$, and green line denotes Fermi level obtained by the DAC method in a self-consistent manner, respectively. Only algebraic decay rate is observed due the failure of Assumption A.

Example 4.5 (Insulating global system, gap assumption invalid for the subsystem). Consider

$$V(x, y) = \begin{cases} -a, & (x, y) \in \{3 < x < 9, 3 < y < 9\}; \\ -b, & (x, y) \in \{[0, 12] \times [0, 12]\} / \{3 < x < 9, 3 < y < 9\}; \\ \text{periodic extension,} & \text{otherwise.} \end{cases}$$



(a) Density difference with DBC (b) Density difference with NBC (c) Density difference with PBC

FIGURE 6. $|\rho(0) - \rho_\Lambda(0)|$ as a function of x in the log-log scale for $\Lambda = [0, 16]$ and a series of enlarged buffer regions $\Lambda_b = [0 - x, 16 + x]$ ($x \geq 0.1$) with different boundary conditions in **Example 4.2**. (a) Density difference with DBC; (b) Density difference with NBC; (c) Density difference with PBC. Algebraic decay rates are observed in all cases due to the failure of Assumption A.

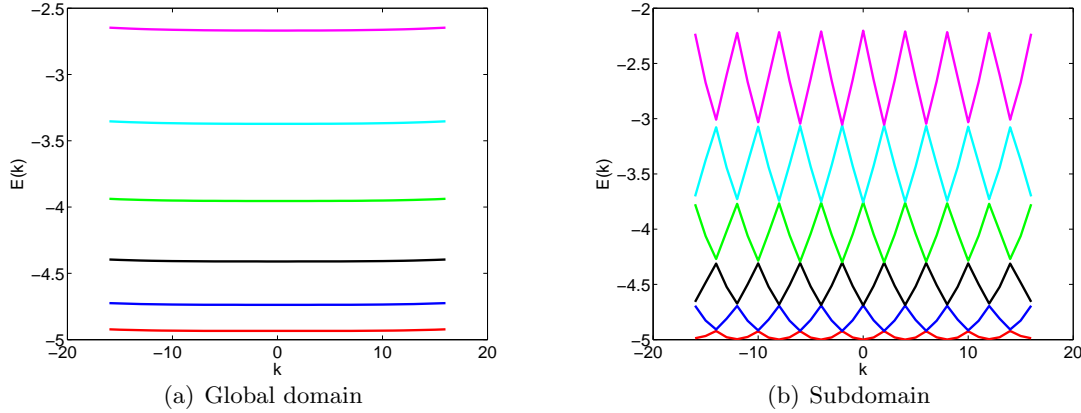


FIGURE 7. Band structures of the global system over $[0, 16]$ and the subsystem over $[0, 8]$ with $a = 5$ and $b = 0$ in **Example 4.3**. (3.9) - (3.10) are valid for the global system while (3.11) is invalid for the subsystem. (a) The global system; (b) The subsystem.

Choose $a = 5$ and $b = 0$ and plot the band structure of this problem in Figure 11(a). It is clear that (3.9)–(3.10) are valid.

Now we fix $\Lambda = [3.1, 8.9] \times [3.1, 8.9]$ and choose $\Lambda_b = [3, 9] \times [3, 9]$. Since $a = -5$, the subsystem is essentially the eigenvalue problem of the Laplacian operator, which implies the invalidity of (3.11). As a consequence, only algebraic decay rate is observed in Figure 12(a). Furthermore, we fix $\Lambda = [5, 7] \times [5, 7]$ and choose a series of enlarged buffer regions $\Lambda_b = [5 - x, 7 + x] \times [5 - x, 7 + x]$ ($x \geq 0.1$) by varying x . $|\rho(5, 5) - \rho_\Lambda(5, 5)|$ as a function of x is shown in Figure 12(b). Algebraic decay rate is also observed again due to the invalidity of (3.11). Finally, we fix $\Lambda = [3, 9] \times [3, 9]$ and choose a series of enlarged buffer regions $\Lambda_b = [3 - x, 9 + x] \times [3 - x, 9 + x]$ ($x \geq 0.1$). $|\rho(3, 3) - \rho_\Lambda(3, 3)|$ as a function of x is shown in Figure 12(c). Exponential decay rate is observed since (3.11) becomes valid in this case.

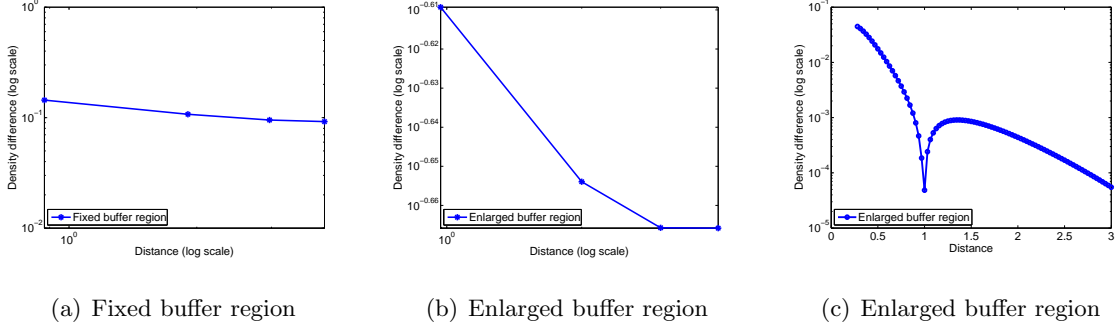


FIGURE 8. Difference between electron densities of the global system and subsystems as a function of distance in **Example 4.3**. (a) $|\rho(x) - \rho_\Lambda(x)|$ with $\Lambda = [0.1, 7.9]$ and $\Lambda_b = [0, 8]$ as a function of x ; (b) $|\rho(5) - \rho_\Lambda(5)|$ with $\Lambda = [3, 5]$ and $\Lambda_b = [3 - x, 5 + x]$ ($x \geq 0.1$) as a function of x ; (c) $|\rho(8) - \rho_\Lambda(8)|$ with $\Lambda = [0, 8]$ and $\Lambda_b = [0 - x, 8 + x]$ ($x \geq 0.1$) as a function of x . Exponential decay rate is observed in (c), while only algebraic decay rates are observed in (a) and (b), due to the validity and invalidity of (3.11) in corresponding cases.

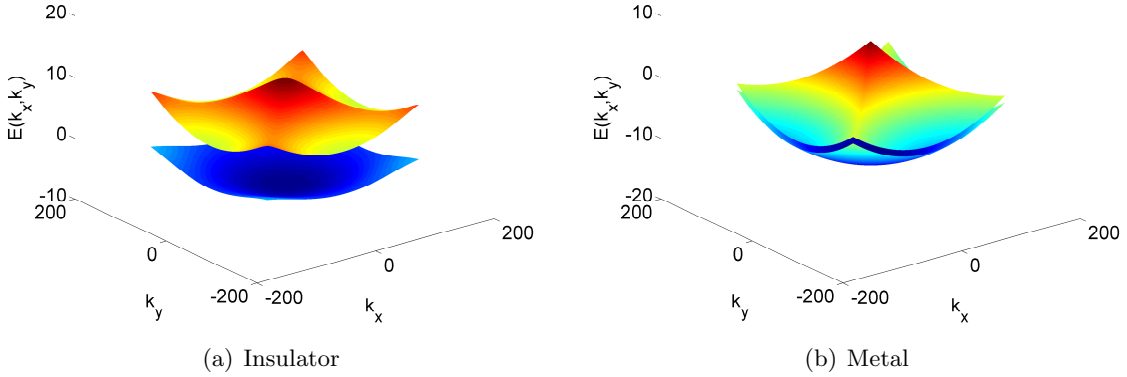


FIGURE 9. Band structures for different parameters in **Example 4.4**. (a) Insulator, where $a = 10$ and $\sigma = 0.15$; (b) Metal, where $a = 10$ and $\sigma = 0.45$.

5. CONCLUSION

In this work, we identify the crucial gap assumption for both the global system and the subsystem for the accuracy of the DAC method for electronic structure calculations. Under the gap assumption, we prove that the pointwise difference between electron densities of the global system and the subsystem decays exponentially as a function of the distance away from the boundary of the subsystem. This analytic conclusion is verified by numerical examples.

From a physical point of view, our result suggests that while the DAC method works quite well for insulating systems, one still needs to be careful in the choice of subdomain and restrictions to guarantee the gap assumption. Moreover, for heterogeneous systems with large local Fermi energy variations, such as metal-insulator-metal bilayer devices or systems involving long range charge transfer, application of the DAC method might need extra care.

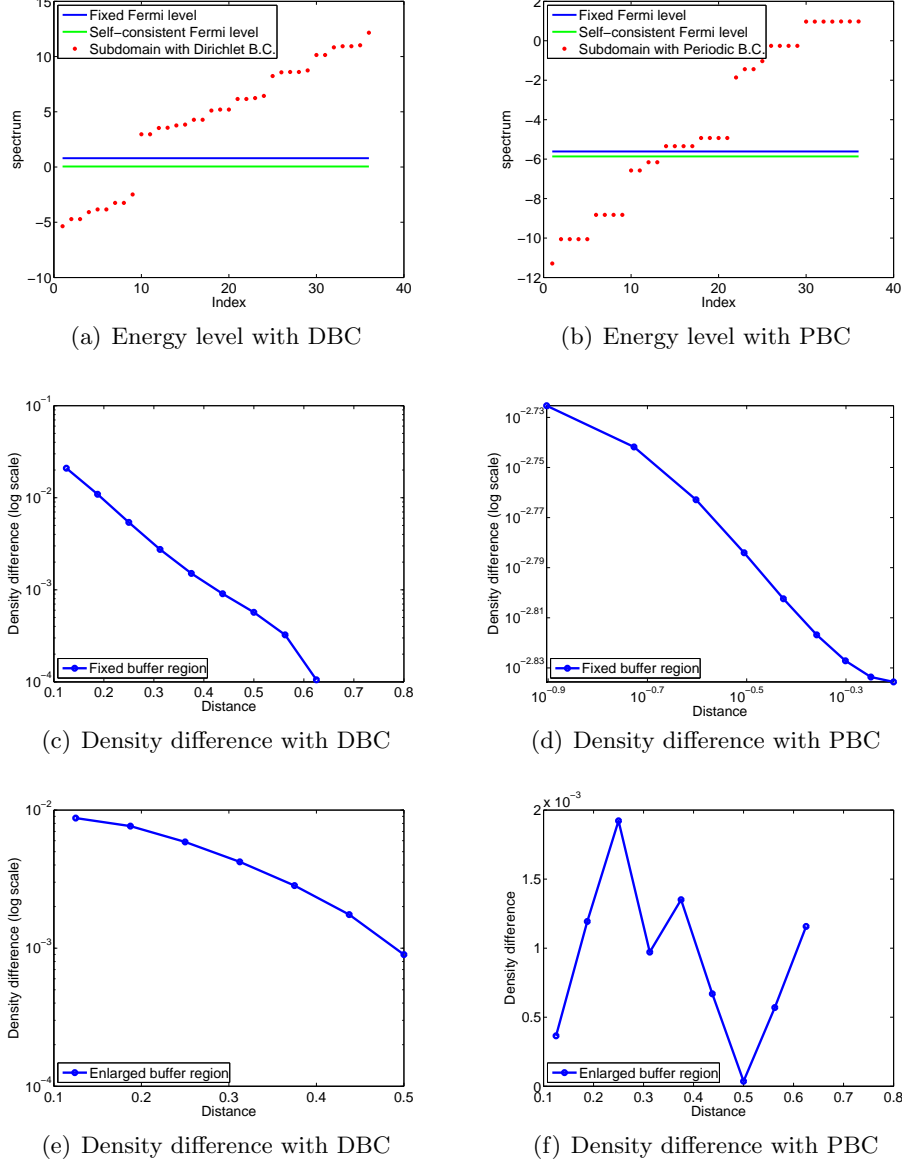


FIGURE 10. Energy levels of the subsystem (top row), $|\rho(x) - \rho_\Lambda(x)|$ with $\Lambda = [0.1, 5.9] \times [0.1, 5.9]$ and $\Lambda_b = [0, 6] \times [0, 6]$ as a function of x (centered row), and $|\rho(2, 2) - \rho_\Lambda(2, 2)|$ with $\Lambda = [2, 4] \times [2, 4]$ and $\Lambda_b = [2 - x, 4 + x] \times [2 - x, 4 + x]$ ($x \geq 0.1$) (bottom row) in **Example 4.4**. Left column: Insulator; Right column: Metal. (a) Energy level with DBC; (b) Energy level with PBC; (c) Density difference with DBC; (d) Density difference with PBC; (e) Density difference with DBC; (f) Density difference with PBC. Decay rates are consistent with theoretical estimates.

Finally, let us emphasize that our accuracy estimate only depends on the size of the gap and the L^∞ norm of the effective potential. Hence, even though the discussion here focuses on the DAC method, the analysis allows for general restriction of Hamiltonian, and hence can be applied to a variety of methods in electronic structure calculations using the domain decomposition idea.

Acknowledgment. We thank Professor Weinan E for suggesting the problem and for his encouragement. J.L. would also like to thank Professor Weitao Yang for helpful discussions. The work

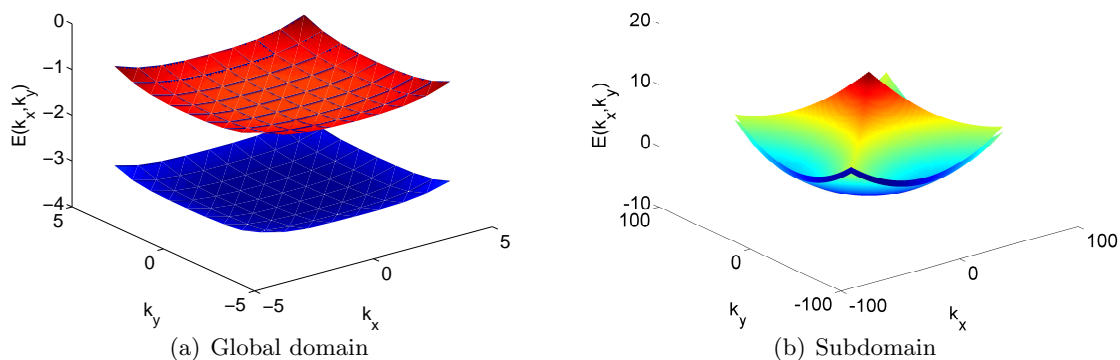


FIGURE 11. Band structures of the global system over $[0, 12] \times [0, 12]$ and the subsystem over $[3, 9] \times [3, 9]$ when $a = 5$ and $b = 0$ in **Example 4.5**. (a) The global system; (b) The subsystem.

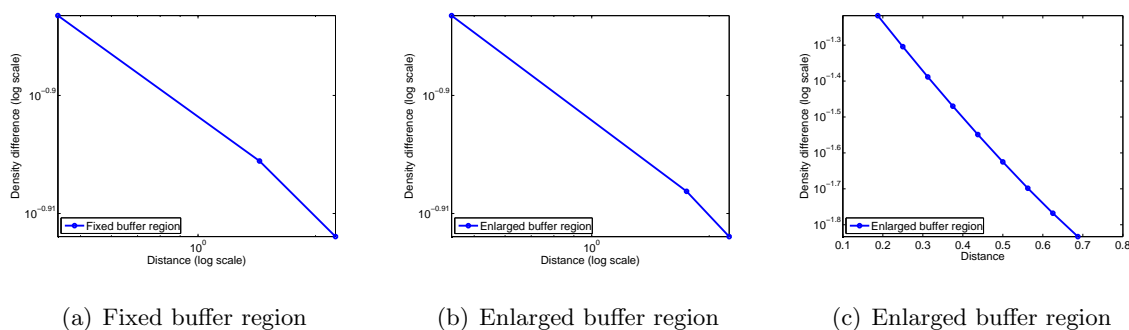


FIGURE 12. Difference between electron densities of the global system and subsystems as a function of distance in **Example 4.5**. (a) $|\rho(x) - \rho_\Lambda(x)|$ with $\Lambda = [3.1, 8.9] \times [3.1, 8.9]$ and $\Lambda = [3, 9] \times [3, 9]$ as a function of x ; (b) $|\rho(5, 5) - \rho_\Lambda(5, 5)|$ with $\Lambda = [5, 7] \times [5, 7]$ and $\Lambda_b = [5 - x, 7 + x] \times [5 - x, 7 + x]$ ($x \geq 0.1$) as a function of x ; (c) $|\rho(3, 3) - \rho_\Lambda(3, 3)|$ with $\Lambda = [3, 9] \times [3, 9]$ and $\Lambda_b = [3 - x, 9 + x] \times [3 - x, 9 + x]$ ($x \geq 0.1$) as a function of x . Exponential decay rate is observed in (c), while only algebraic decay rates are observed in (a) and (b) due to the validity and invalidity of (3.11) in corresponding cases.

of J.C. was supported in part by the National Science Foundation via grant DMS-1217315. The work of J.L. was supported in part by the Alfred P. Sloan Foundation and the National Science Foundation under grant no. DMS-1312659.

REFERENCES

- [1] S. Agmon, *On kernels, eigenvalues, and eigenfunctions of operators related to elliptic problems*, Comm. Pure Appl. Math. **18** (1965), 627–663.
- [2] M. Aizenman, A. Elgart, S. Naboko, J. H. Schenker, and G. Stolz, *Moment analysis for localization in random Schrödinger operators*, Invent. Math. **163** (2006), 343–413.
- [3] M. Barrault, E. Cancés, W.W. Hager, and C. Le Bris, *Multilevel domain decomposition for electronic structure calculations*, J. Comp. Phys. **222** (2007), 86–109.

- [4] G. Bencteux, M. Barrault, E. Cancés, W. W. Hager, and C. Le Bris, *Domain decomposition and electronic structure computations: A promising approach*, Numerical analysis and scientific computing for PDEs and their challenging applications, 2008, pp. 147–164.
- [5] M. Benzi, P. Boito, and N. Razouk, *Decay properties of spectral projectors with applications to electronic structure*, SIAM Review **55** (2013), 3–64.
- [6] D. R. Bowler and T. Miyazaki, *Calculations of millions of atoms with density functional theory: linear scaling shows its potential*, J. Phys.: Condens. Matter **22** (2010), 074207.
- [7] W. E and J. Lu, *The electronic structure of smoothly deformed crystals: Wannier functions and the Cauchy-Born rule*, Arch. Ration. Mech. Anal. **199** (2011), 407–433.
- [8] W. E and J. Lu, *The Kohn-Sham equation for deformed crystals*, Mem. Amer. Math. Soc. **221** (2013).
- [9] C. J. García-Cervera, J. Lu, Y. Xuan, and W. E, *Linear-scaling subspace-iteration algorithm with optimally localized nonorthogonal wave functions for Kohn-Sham density functional theory*, Phys. Rev. B **79** (2009), 115110.
- [10] S. Goedecker, *Linear scaling electronic structure methods*, Rev. Mod. Phys. **71** (1999), 1085–1123.
- [11] P. Hohenberg and W. Kohn, *Inhomogeneous electron gas*, Phys. Rev. **136** (1964), B864–B871.
- [12] M. Kobayashi and H. Nakai, *Divide-and-conquer-based linear-scaling approach for traditional and renormalized coupled cluster methods with single, double, and noniterative triple excitations*, J. Chem. Phys. **131** (2009), 114108.
- [13] W. Kohn, *Density functional and density matrix method scaling linearly with the number of atoms*, Phys. Rev. Lett. **76** (1996), 3168–3171.
- [14] W. Kohn and L. J. Sham, *Self-consistent equations including exchange and correlation effects*, Phys. Rev. **140** (1965), A1133–A1138.
- [15] R. M. Martin, *Electronic structure: Basic theory and practical methods*, Cambridge University Press, 2004.
- [16] N. Ohba, S. Ogata, T. Kouno., T. Tamura, and R. Kobayashi, *Linear scaling algorithm of real-space density functional theory of electrons with correlated overlapping domains*, Comput. Phys. Commun. **183** (2012), 1664–1673.
- [17] R. Parr and W. Yang, *Density-functional theory of atoms and molecules*, International Series of Monographs on Chemistry, Oxford University Press, New York, 1989.
- [18] E. Prodan and W. Kohn, *Nearsightedness of electronic matter*, Proc. Natl. Acad. Sci. **102** (2005), 11635–11638.
- [19] F. Shimojo, R. K. Kalia, A. Nakano, and P. Vashishta, *Divide-and-conquer density functional theory on hierarchical real-space grids: Parallel implementation and applications*, Phys. Rev. B **77** (2008), 085103.
- [20] F. Shimojo, S. Ohmura, A. Nakano, R.K. Kalia, and P. Vashishta, *Large-scale atomistic simulations of nanostructured materials based on divide-and-conquer density functional theory*, Eur. Phys. J. Spec. Top. **196** (2011), 53–63.
- [21] L.-W. Wang, Z. Zhao, and J. Meza, *Linear-scaling three-dimensional fragment method for large-scale electronic structure calculations*, Phys. Rev. B **77** (2008), 165113.
- [22] W. Yang, *Direct calculation of electron density in density-functional theory*, Phys. Rev. Lett. **66** (1991), 1438–1441.
- [23] W. Yang, *Direct calculation of electron density in density-functional theory: Implementation for benzene and a tetrapeptide*, Phys. Rev. A **44** (1991), 7823–7826.
- [24] W. Yang and T.-S. Lee, *A density-matrix divide-and-conquer approach for electronic structure calculations of large molecules*, J. Chem. Phys. **103** (1995), 5674–5678.
- [25] Z. Zhao, J. Meza, and L.-W. Wang, *A divide-and-conquer linear scaling three-dimensional fragment method for large scale electronic structure calculations*, J. Phys.: Condens. Matter **20** (2008), 294203.

MATHEMATICS DEPARTMENT, SOUTH HALL 6705, UNIVERSITY OF CALIFORNIA, SANTA BARBARA, CA 93106
E-mail address: cjr@math.ucsb.edu

DEPARTMENTS OF MATHEMATICS, PHYSICS, AND CHEMISTRY, DUKE UNIVERSITY, BOX 90320, DURHAM, NC 27708

E-mail address: jianfeng@math.duke.edu